ARTICLE

Development of a microfluidic platform for the encapsulation of baker's yeast *Saccharomyces cerevisiae* in alginate hydrogel microparticles

Alexandra Melise D. Hulog[*¶1,2], Miguel Francisco Jose P. Ordoñez[¶1], Noel A. Oquendo[2], Mariane Desiree C. Avendaño[3], Jamielyn N. Kaw[2], Alwin Darren O. Dagdag[2], and Ricardo Jose S. Guerrero[1,4]

[1]Ateneo Research Institute of Science and Engineering, School of Science and Engineering, Ateneo de Manila University, Katipunan Avenue, 1108 Quezon City, Philippines
[2]Department of Chemistry, School of Science and Engineering, Ateneo de Manila University, Katipunan Avenue, 1108 Quezon City, Philippines
[3]Department of Physics, School of Science and Engineering, Ateneo de Manila University, Katipunan Avenue, 1108 Quezon City, Philippines
[4]Department of Electronics, Computer, and Communications Engineering, School of Science and Engineering, Ateneo de Manila University, Katipunan Avenue, Quezon City, 1108, Philippines

[¶]These authors contributed equally to this manuscript.

ABSTRACT

The encapsulation of cells in a semi-permeable polymer matrix enables the simulation of biochemical microenvironments for studying cellular response and interactions with minimal reagent use. Traditional methods often lack reproducibility, leading to variations in encapsulation quality. In contrast, microfluidic techniques can rapidly and consistently produce hydrogel microstructures encapsulating living cells. However, the fabrication of these devices remains challenging due to high initial costs and facility requirements. To address this, a microfluidic platform was developed using a CNC milling machine to enhance the accessibility of microfluidic-based cell encapsulation in hydrogel microstructures.

A flow-focusing droplet generator was designed and employed to generate alginate-in-oil droplets containing baker's yeast cells. The microfluidic device was fabricated from PMMA using CNC milling and sealed via solvent-assisted bonding, ensuring accessibility and ease of production compared to traditional lithography-based fabrication methods. The optimized system operated at a 400:4 oil-to-alginate phase flow rate, generating monodisperse alginate droplets at 10 Hz. The droplets were subsequently gelated in calcium chloride to form alginate microparticles. The resulting microparticles, averaging 164.14 ± 15.11 µm in the Feret diameter along the major axis, exhibited controlled morphology, with predominantly teardrop and oval shapes. Imaging confirmed the presence of multiple spherical-

*Corresponding author
Email Address: ahulog@ateneo.edu
Date received: 27 December 2024
Dates revised: 29 January 2025; 02 June 2025
Date accepted: 06 July 2025
DOI: https://doi.org/10.54645/202518SupDSK-64

KEYWORDS

encapsulation, *Saccharomyces cerevisiae*, alginate, microfluidics, droplet generator, cell biology

ovoid yeast cells within the resulting hydrogels, verifying successful encapsulation. The findings support the feasibility of using CNC-milled microfluidic platforms for controlled and reproducible yeast encapsulation in hydrogel matrices, demonstrating their potential for broader biological and biotechnological applications.

INTRODUCTION

Cell microencapsulation involves the isolation of functional cells within the confines of a semi-permeable polymeric membrane. Immobilization via this technique prevents premature cell death as an effect of changes in the cell's environment (Choudhary et al. 2016). These methods have been used to study cell growth and viability for several use cases, such as tissue engineering (Karaca et al. 2023) and transplantation (Gasperini et al. 2014). Additionally, cell encapsulation produces a simulated microenvironment which makes cell responses and interactions easier to observe, especially when treated with different stimuli (Rivera-Tarazona et al. 2021). Non-mammalian cells, such as yeast and *Escherichia coli*, are generally more robust than their mammalian counterparts while also being sensitive to stimuli, thus making them ideal for these types of cellular response and interaction studies (Inda & Lu 2020). *Saccharomyces cerevisiae* (baker's yeast) was selected as a model encapsulation target due to its large size relative to other readily available bacterial cells and its ability to survive more drastic environmental changes (Rivera-Tarzona et al. 2020).

Hydrogels are suitable for cell encapsulation since they provide a semi-permeable structure that isolates the cells while allowing the diffusion of vital substances (Bonani et al. 2020). Various matrices, such as chitosan, gelatin, and hyaluronic acid have been explored for their ability to encapsulate cells while retaining their microstructure (Hamilton et al. 2021; Khayambashi et al. 2021; Mohanto et al. 2023). Alginate, a polysaccharide derived from brown algae, has been studied intensively as an appropriate material for producing biocompatible hydrogels, due to its gelling abilities, as well as its non-toxic nature (Tomić et al. 2023).

Various methods have been developed for producing alginate-based hydrogel beads, including batch emulsion, spray-drying, and extrusion (Ahn & Kim 2015; Hoesli et al. 2012; Serp et al. 2000). However, these methods often produce polydisperse microparticles which compromise reproducibility. Achieving monodispersity is crucial in maintaining control over reaction conditions and accuracy in tuning conditions that may affect the encapsulated cells (Schneider et al. 2013). For cell studies, monodispersity allows droplets to act as reproducible bioreactors wherein cells can be analyzed in parallel to one another (Giuliano 2020). To achieve this, droplet-based microfluidics has been explored for its highly controllable and reproducible synthesis methods that allow for the precise control of the microparticle size distribution. This can be done by manipulating the design of the microfluidic device and the conditions of the immiscible input fluids.

Microfluidic devices for microparticle production are commonly fabricated via soft lithography (Ren et al. 2013; Zhang et al. 2021). However, the equipment and facilities required to reproduce these methods are generally difficult to procure and scale up. Thus, despite its cost-effectiveness and compatibility with diverse materials, the use of soft lithography for high-precision and large-scale applications is limited (Xu et al. 2025). In contrast, milling has become the preferred fabrication technique for several microfluidic devices. A computer numerical control (CNC) machine can remove a considerable amount of material in a short amount of time, making it effective in carving out channels, through holes, and chambers to create the microfluidic device. Additionally, CNC milling machines integrate well with computer-aided design (CAD) and computer-aided manufacturing (CAM) software to reduce human errors in manufacturing the device while increasing speed and convenience (Brousseau et al. 2010; Guckenberger et al. 2015; Scott & Ali 2021). While microfluidic devices can be manufactured out of a variety of materials, poly(methyl methacrylate) (PMMA) was chosen due to its low cost, high accessibility, and general ease of fabrication (Ren et al. 2013).

Using designs adapted from our previous work on the encapsulation of *E. coli* and the fabrication of microfluidic devices, we have developed a process using CNC milling methods for the real-time imaging of alginate-in-oil droplet generation. These droplets were gelated with calcium chloride to produce alginate microparticles. The method was further adapted for the encapsulation of *Saccharomyces cerevisiae* (baker's yeast) in the hydrogel matrix. Imaging was performed to determine the size of the microparticles and the success of cell encapsulation. This study, therefore, opens opportunities for research on cell encapsulation which may otherwise be cost-prohibitive or inaccessible.

MATERIALS AND METHODS

Materials

Span 80 was obtained from Merck (Darmstadt, Germany). Mineral oil (light USP grade), sodium alginate (food grade), and calcium chloride (flakes, 74%, technical grade) were obtained from Dalkem Corporation (Quezon City, Philippines). Baker's yeast (Angel Yeast, China) was used for encapsulation and was obtained from a local vendor. The microfluidic droplet generators were fabricated using 2 mm- thick poly(methyl methacrylate) (PMMA) plates (Superfab Inc., Philippines). 70% ethanol (RCI Labscan, Philippines) was prepared for solvent-assisted bonding via hydraulic press. Polytetrafluoroethylene (PTFE) tubing (AS ONE, Japan) with 1.6 mm x 0.8 mm OD/ID was used to connect the microfluidic device to the rest of the experimental setup.

Design and fabrication of microfluidic droplet generator

Microfluidic droplet generators generally consist of a two-phase flow system of immiscible liquids flowing at different volumetric flow rates and meeting at a junction with specific geometry. The viscous forces imparted by the fast-moving continuous phase onto the slower-moving dispersed phase cause the latter to shear apart into uniformly sized droplets in a controlled, recurring manner, forming a monodisperse emulsion. Systems with additional phases can be used to create higher order emulsions or tunable micromixers at a droplet level (e.g. double emulsions, triple emulsions, two-component aqueous mixtures in organic carrier fluid, etc.) (Moragues et al. 2023). For two-phase systems, a series of channels guides the two phases to one of three types of junctions: a perpendicular cross-flow t-junction, a flow-focusing junction, or a co-axial/co-flow configuration (Sadasivan et al. 2025). T-junctions are the simplest geometry, involving a straight channel containing the continuous phase and a dispersed phase of a lower volumetric flow rate which enters the straight channel from a perpendicular side channel. Flow-focusing junctions feature a straight channel for the slower dispersed phase, which is pinched by the continuous phase from two adjoining, often perpendicular, side channels, as they enter a narrow orifice towards the outlet of the junction. Co-flow droplet generators feature a co-axial geometry where a capillary or small-diameter tube carrying the dispersed phase is placed inside a larger-diameter tube carrying the continuous phase, imparting a uniform circumferential shear force onto the dispersed phase.

In this study, a flow-focusing channel geometry was used (Fig. 1). The flow-focusing droplet generator geometry involves six key dimensions: continuous phase inlet width (W_c), dispersed phase inlet width (W_d), orifice width (W_{or}), orifice length (L_{or}), outlet width (W_{out}), and channel height (H). This process was aided by modeling using the Design Automation of Fluid Dynamics (DAFD) tool developed by the Cross-disciplinary Integration of Design Automation Research (CIDAR) Lab at Boston University (Lashkaripour et al. 2019; McIntyre et al. 2023). CAD models were prepared using Autodesk Fusion 360, and toolpaths were designed and exported to machine code using the Fusion 360 CAM package. The channels were machined onto one side of the PMMA plates using a Nomad 3 Desktop CNC Milling Machine (Carbide 3D, USA). On the opposite face, ports were machined based on a microfluidic chip interconnection port design by Pfreundt et al. (2015). These ports are designed to accept 1.6 mm x 0.8 mm OD/ID PTFE tubing, taking the place of HPLC fittings and ferrules commonly used in similar microfluidic device designs. The droplet generators were scrubbed clean with soap and dried using compressed air, then inspected under the microscope for debris and dimensional accuracy. The chips were then sealed using a methodology based on the work of Liga et al. (2016), which involves solvent-assisted bonding of PMMA to PMMA in a 10-ton hydraulic press with heated platens. The hydraulic press plates were pre-heated to 70°C. Immediately before the bonding process, the PMMA plates were wiped clean with a dust-free wipe (Kimtech, USA) soaked with 70% ethanol and wiped dry. To prepare the surfaces for bonding, 80 µL of 70% ethanol was then dispensed onto a blank piece of PMMA, then the milled droplet generator was placed on top, with the open channels in contact with the ethanol. This was then placed into the hydraulic press, and compressed at 0.5 MPa for 5 minutes. Excess ethanol in the channels was cleared using compressed air.

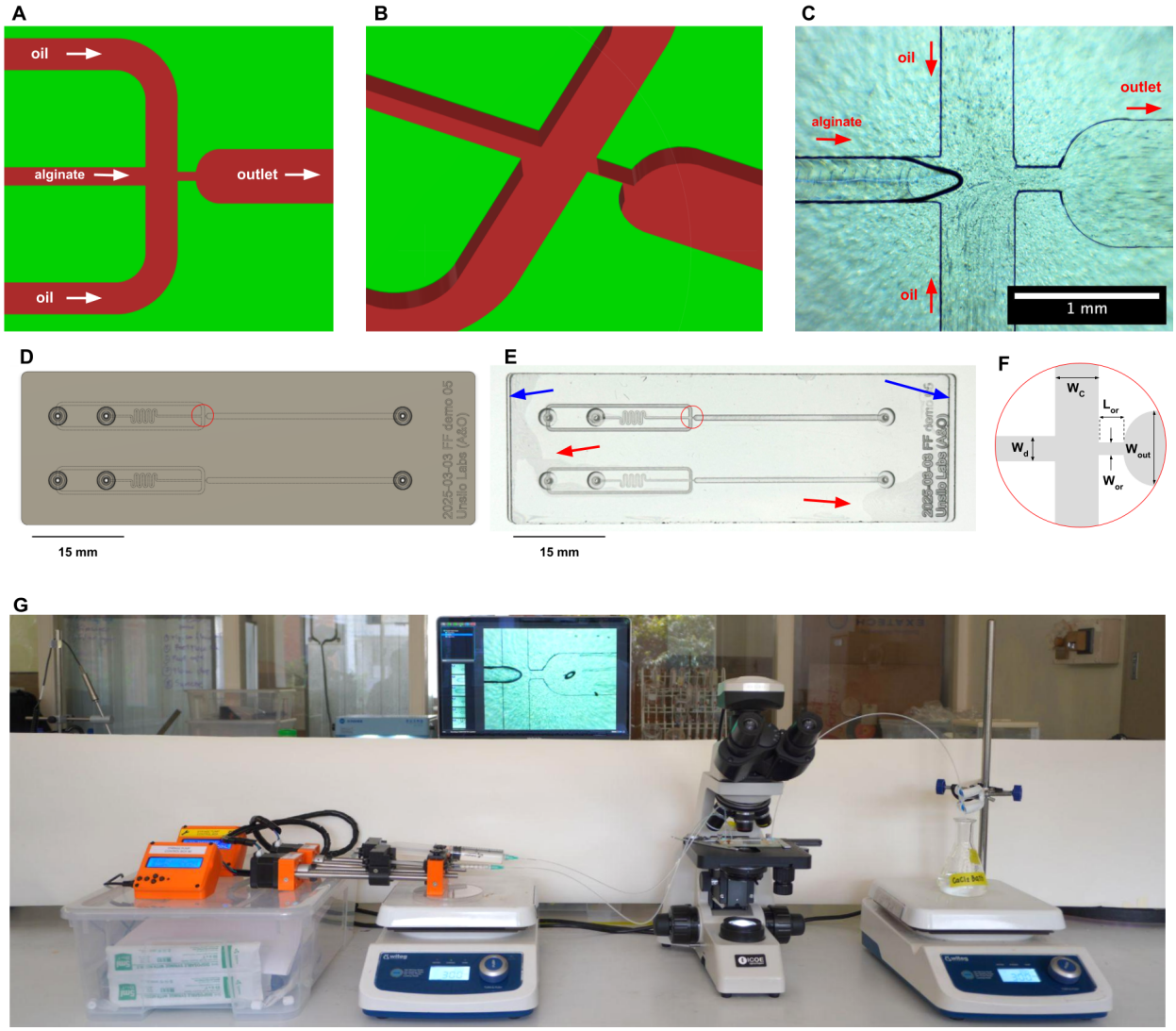

Figure 1: Multiple views of the droplet generation setup. (A-B) Top-down and isometric views of flow-focusing junction from CAD model in Autodesk Fusion 360. (C) Micrograph of the junction in use. Red arrows indicate flow direction. (D) CAD model of the full device (75 mm x 25 mm) with two independent droplet generators. Each generator has three ports which accept PTFE tubing (1.6 mm x 0.8 mm). A continuous phase (oil) inlet and dispersed phase (alginate) inlet feed into a cross-junction for droplet generation. (E) Image of assembled droplet generator, taken using a mobile phone camera at distance to avoid parallax error. This device was machined out of PMMA (t = 2 mm) using a CNC milling machine, then sealed onto a blank PMMA slide via solvent-assisted heated press bonding. Red arrows indicate regions with possible incomplete bonding, and blue arrows indicate slight misalignment. Neither of these factors affected the droplet generation experiments. (F) Detailed view of encircled regions in Fig. 1D & 1E showing flow focusing junction. Channel dimensions are indicated: dispersed phase inlet width (W_d), continuous phase inlet width (W_C), orifice width (W_{or}), orifice length (L_{or}), and outlet width (W_{out}). (G) A photo of the experimental set-up consisting of (L-R): two 3D-printed open-source syringe pumps based on designs adapted from Samokhin (2020). The syringes contain: 1) mineral oil with Span 80; 2) yeast cells suspended in a sodium alginate solution with a small stir bar for constant agitation over a magnetic stir plate. The syringes are connected to the microfluidic droplet generator via PTFE tubing. The microfluidic device is positioned under a trinocular microscope for monitoring and data collection, and the outlet tubing of the droplet generator leads to a calcium chloride crosslinking bath under constant agitation.

Generation of alginate microparticles

The oil phase consisted of 0.1% (w/v) Span 80 in mineral oil. Removal of debris and air bubbles was done with the use of a syringe filter (pore size: 0.45 µm) and a sonication bath. The solution was loaded into a 50 mL gas-tight syringe (Trajan Scientific). The aqueous phase consisted of 1% (w/v) sodium alginate dissolved in deionized water. A syringe filter (pore size: 0.45 µm) was used to remove any undissolved debris. For alginate with yeast, a 1% (w/v) stock yeast solution was prepared with sucrose and deionized water. Using a hemocytometer, it was determined that the cell count for the stock solution was 2,940 cells/µL. In order to achieve single-cell encapsulation for the droplet size used in this study ($V_{droplet}$ = 1.77 nL), a cell count of 55 cells/µL was targeted (Macosko et al. 2015; Collins et al. 2015). From the stock solution, 50 µL of the cell suspension was diluted with 10 mL of the filtered alginate solution, and vortex mixed for even distribution of the cells. The aqueous phase was loaded into a 1 mL syringe containing a small magnetic stir bar.

The experimental setup was prepared (**Fig. 1G**), starting by loading the syringes into 3D-printed syringe pumps. The pumps were fabricated and tested beforehand using designs adapted from Samokhin (2020). PTFE tubing was connected to the syringes, and the syringe pumps were manually advanced to fill the tubing and evacuate air and debris. The microfluidic device was placed on the ICOE BM38T trinocular microscope stage, and the tubing was connected to the ports. The end of the outlet tubing was attached to a waste beaker for the initial priming of the system. A key step in the preparation process is the initial filling of the microfluidic channels, as wetting issues can occur if the proper sequence of initial flow is not observed. The syringe pump with the oil syringe was initially set to 100uL/min during the priming process to allow the oil to enter the chip first. This ensures that the oil inlet channels, orifice, and outlet are fully wetted. In order to maintain close control of the alginate phase meniscus, the respective alginate-phase syringe pump was actuated manually. This prevented backflow as pressure built up from the oil phase, while also preventing the alginate phase from flowing too quickly and wetting the chip ahead of the oil. An air bubble was trapped between the alginate inlet channel and the flow-focusing junction, which was slowly pushed out of the chip until the alginate phase reached the junction. When a stable dripping droplet formation regime was established, the oil-phase syringe pump flow rate was increased to the final 400 µL/min setting, and the manual alginate priming process was repeated. Once stable dripping-regime droplet formation was achieved for this flow rate, the alginate-phase syringe pump was then started at 4 µL/min. The system was left to stabilize for three minutes before confirming on-chip droplet generation in real-time via optical microscopy. In addition, droplets were observed to be exiting the outlet tubing into the waste beaker. Afterwards, the end of the outlet tubing was then quickly transferred to an Erlenmeyer flask containing 2% (w/v) calcium chloride crosslinking bath under constant agitation at 300 RPM. The tip of the outlet tubing was submerged approximately 5-10 mm below the surface of the solution to aid in crosslinking. Once the droplet collection was completed, the outlet tubing was removed from the crosslinking bath, and the bath was stirred for 30 minutes to ensure gelation.

The crosslinking bath was washed with filtered calcium chloride solution and centrifuged (2236R High-Speed Centrifuge, Gyrozen Co., Ltd., China) at 630 x g for 10 minutes. Excess liquid was removed with the use of a 50 mL serological pipette to minimize loss of product. This washing step was repeated once again with calcium chloride and twice with deionized water. The bottom layer of the washing was collected for imaging of the microparticles.

Imaging

Initial imaging of the microparticles was done using an ICOE BM38T Biological Microscope with trinocular attachment to accommodate an ICOE HDCE-X5N 5MP USB 2.0 Digital Camera. Standard achromatic objectives 10x/0.25 (W.D. = 5.8 mm) and 40x/0.65 (W.D not listed, approx. 0.3 mm) were used alongside 1W LED single-point illumination source. Two 24x24 mm coverslips were placed on the edges of a microscope slide to act as vertical spacers. After addition of two droplets containing microparticles in the center of the slide, a 24x50 mm coverslip was placed with the ends overlapping those placed on the edges. This allowed liquid to spread across the surface of the slide while minimizing the deformation of the hydrogel microparticles.

For imaging of droplet formation during generation, a smartphone camera was coupled to a microscope and used to record at 240 frames per second (FPS). This setup allowed for the capturing of high-speed video footage of the dynamic formation process.

For microbead imaging, counting, and shape analysis, we developed a microfluidic chip design that enabled size-based filtering and separation, as described in the Supplementary Information (Fig. S1) and adapted from a design by Velders (2023). Crosslinked microparticles suspended in the crosslinking bath solution flowed through this chip and were imaged using a microscope to facilitate bead characterization under controlled flow conditions.

Data analysis

A sample size of n = 50 was used for microparticle analysis. Distinct particles in micrographs taken at 10x magnification were analyzed using ImageJ, an image processing software, as described in the Supplementary Information (Fig. S2). The software's "Analyze Particle" function was used to determine the size and circularity of individual particles.

For dynamic droplet analysis, a custom image processing pipeline was developed and applied to high-speed videos (240 FPS) captured via smartphone microscopy. The code automatically extracted droplet size and tracking on a frame-by-frame basis within a user-defined region of interest and time window (Fig. S3). It applied OpenCV object tracking and Hough Circle Transform analysis to detect and measure droplets across frames. Output CSV files with raw measurements and basic statistical data were generated alongside annotated snapshots to aid in verification and downstream analysis. Full pseudocode and implementation details are provided in the Supplementary Information (Fig. S3-S5).

RESULTS AND DISCUSSION

Fabrication of microfluidic device

PMMA microfluidic droplet generators were successfully fabricated via micromachining and solvent-assisted bonding. The critical dimensions of the milled microfluidic droplet generator were measured and compared to those specified in the CAD models (**Fig. 1D-E**). As reported in Table 1, the geometries were accurately milled and only had minimal deviations from the dimensions specified in the CAD model. The small discrepancies between the dimensions in the CAD models and milled droplet generator can be attributed to multiple factors during the fabrication process including the mechanical resolution and repeatability specifications of the CNC mill, as well as the wear and deterioration of the end mills used. However, none of these discrepancies interfered with the ability of the microfluidic droplet generator to produce droplets in a consistent and controlled manner.

Table 1: Comparison of the designed and actual microfluidic droplet generator dimensions (n=1)

Key Dimensions	Design (µm)	Actual (µm)	Error (%)
Continuous phase inlet width (W_c)	525	515	1.80
Dispersed phase inlet width (W_d)	302	296	2.14
Orifice width (W_{or})	151	151	0.00
Orifice length (L_{or})	300	307	1.67
Outlet width (W_{out})	900	879	2.31

Formation of alginate droplets

Alginate droplets were generated using the microfluidic droplet generators at a 100:1 oil to aqueous phase flow rate ratio as shown in **Fig. 2**. The flow rates for the oil and aqueous phases used were 400 and 4 µL/min, respectively. At these flow rates, stable droplet formation occurred and an average alginate droplet diameter of 175.46 ± 8.88 µm was achieved. Balancing the droplet generation rate and the droplet generator and interconnect system integrity is critical in optimizing the system's throughput and maintaining stable droplet formation. Lower flow rates, particularly for the oil phase, produced larger droplets that would be less likely to result in single cell encapsulation. Additionally, the droplets would move slowly in the viewing chamber, causing them to merge when their boundaries came in contact. While it is generally desirable to increase the flow rates to increase the system's throughput, exceeding the operational limits of the microfluidic device, particularly the ports, can compromise chip integrity, negatively impact droplet stability, and consequently produce polydisperse droplets. Use of the selected flow rates resulted in higher volume output and droplet diameters approaching the target size desired for possible single cell encapsulation, best seen in Table S1. Chip design can be further refined for higher flow rates to ensure chip integrity, particularly to prevent the popping out of plugs from the ports due to high pressure build up in the generator.

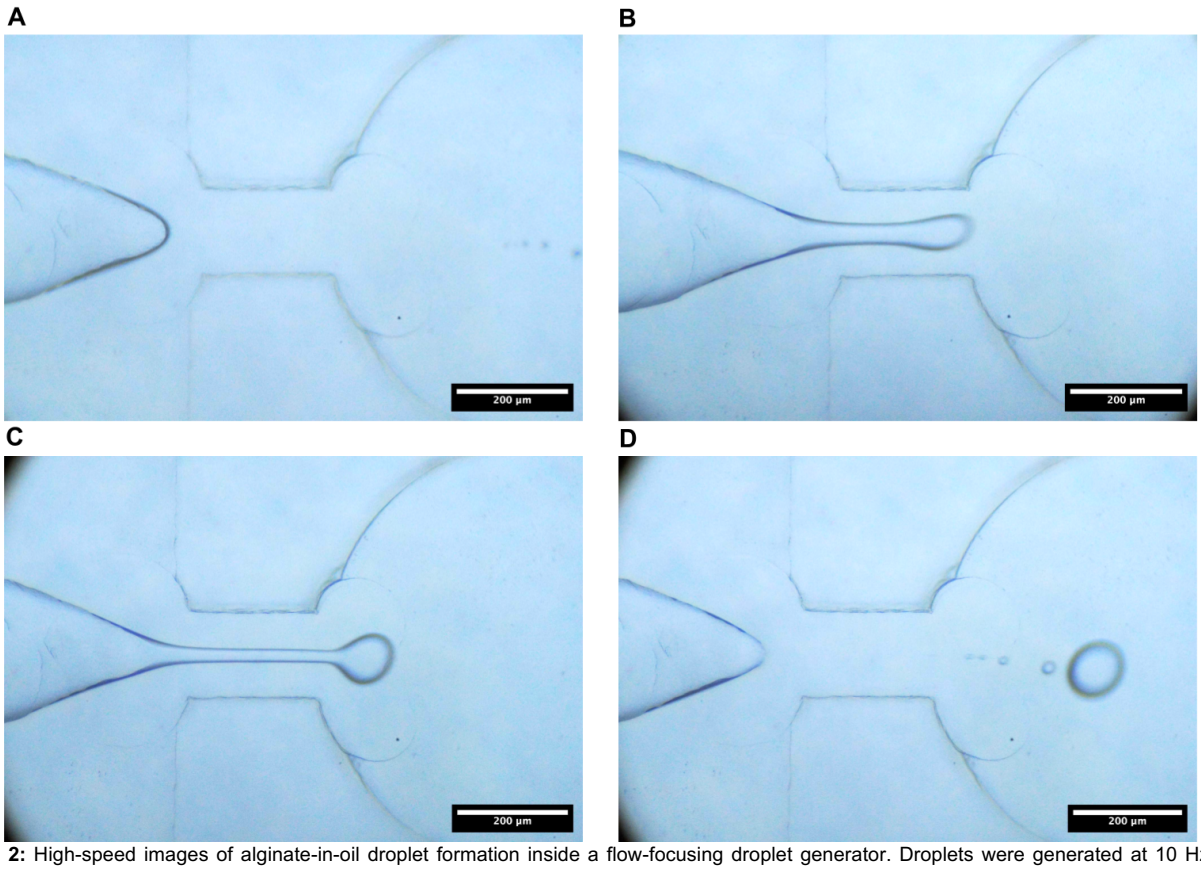

Figure 2: High-speed images of alginate-in-oil droplet formation inside a flow-focusing droplet generator. Droplets were generated at 10 Hz, with volumetric flow rates of Q_{oil} = 500 µL/min and $Q_{alginate}$ = 5 µL/min, passing through a 150-µm orifice. (A) Starting phase of droplet formation, where the alginate solution (leftmost) forms a v-shaped fluid front due to the oil phase flowing from the top and bottom, with both fluids approaching the outlet towards the right. (B) Alginate solution begins to fill the orifice region, compressed and isolated to the center of the channel by the high flow rate oil phase. (C) The alginate solution begins to exit the end of the 150-µm orifice into a much wider 900-µm outlet channel. The drastic changes in channel width and the resulting shear forces provide a mechanism for consistent droplet break-up, as evidenced by the necking of the alginate flow. (D) The alginate in the outlet channel detaches from the main inlet flow, and a droplet is formed. The alginate fluid front returns to the center of the junction as seen in Fig. 2A. The newly-formed droplet (d = 101 µm) can be seen in the outlet channel, with satellite droplets (largest d = 26 µm) trailing close behind. Satellite droplets are regularly seen in microfluidic droplet generators and are generated with a consistent size and quantity for a given experimental condition (flow rate, emulsion system, channel geometry). They can be collected or discarded as needed using microfluidic flow splitting or off-chip filtration of the final product, the latter of which was conducted in this study.

Characterization of alginate microparticles

Additional size measurements using the microfluidic particle size separator (Fig. S6) along with measurement of the Feret diameters to accommodate for non-spherical particles yielded an average bead diameter of 161.14 ± 15.11 µm on the major axis, and 88.78 ± 48.71 µm on the minor axis (Table S1) for crosslinked alginate particles with yeast cells. Majority fell in the 141.822 to 171.822 µm range, as seen in **Fig. 3** and summarized in Table S2. The larger particles can be attributed to the occasional merging of droplets either on chip or in the outlet tubing. When compared to the diameters of the on-chip generated droplets, a reduction in the size of most microparticles is apparent. Slight shrinking tends to occur in hydrogels during the crosslinking process due to interaction of formed bonds (Łabowska, 2023). The crosslinked microparticles had variations in morphology, with teardrop and oval-shaped ones being the most prominent, as evident in **Fig. 4A and 4C**. The calculated average microparticle circularity was 0.879 ± 0.023. Circularity is used in place of sphericity when the exterior surface areas cannot be accurately measured. However, the sphericity value is normally 10-20% less than the circularity value when used to analyze non-spheroid particles (Grace & Ebneyamini 2021). Deviations between the shape and size of on-chip droplets and hydrogel microparticles were likely due to the high flow rates used for droplet generation. Rapid dropping into the crosslinking bath caused elongation of the hydrogel microparticles as they reacted with calcium chloride (Hu et al. 2012). A schematic diagram in **Fig. 5** shows an overview of the role of crosslinking in the encapsulation of the yeast cells within the alginate. The exchange of cations between calcium chloride and sodium alginate enables calcium chloride to serve as an ionic crosslinker that produces calcium alginate hydrogels within seconds (Łabowska et al. 2023; Savić Gajić et al. 2023). With the presence of the crosslinker, the droplets therefore solidify into hydrogels.

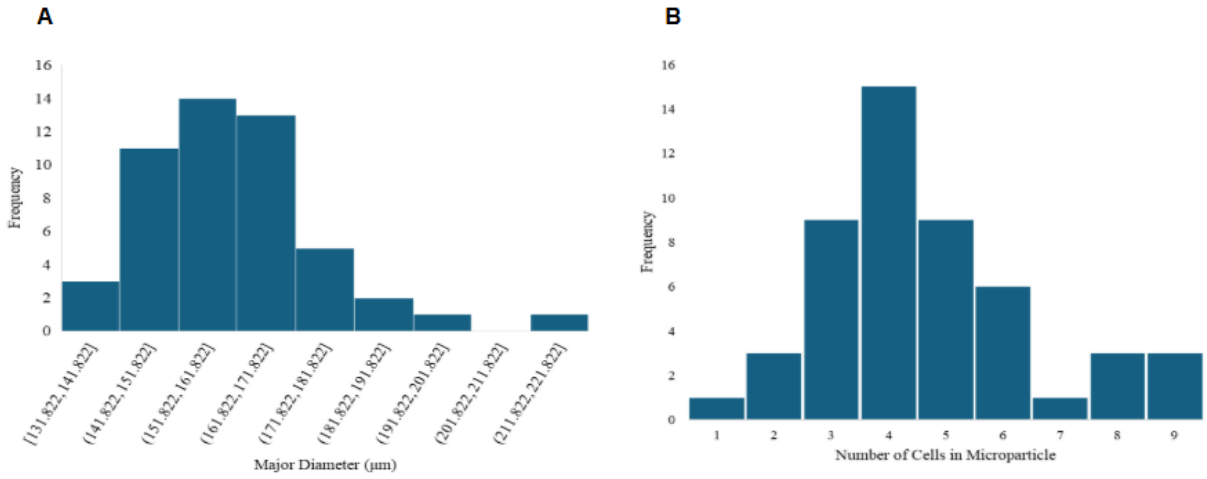

Figure 3: Histograms of (A) crosslinked alginate with yeast microparticles' major Feret diameters. Majority of the microparticles only had a slight deviation from the characterized on-chip droplet size. The presence of larger microparticles can be attributed to slight disturbances to the setup, particularly to the inlet tubings, causing droplet merging. (B) Encapsulated yeast cells in crosslinked alginate microparticles. While dilutions were conducted, vortexing proved to be an inadequate method of mixing the cells in the alginate phase due to the solution's higher viscosity.

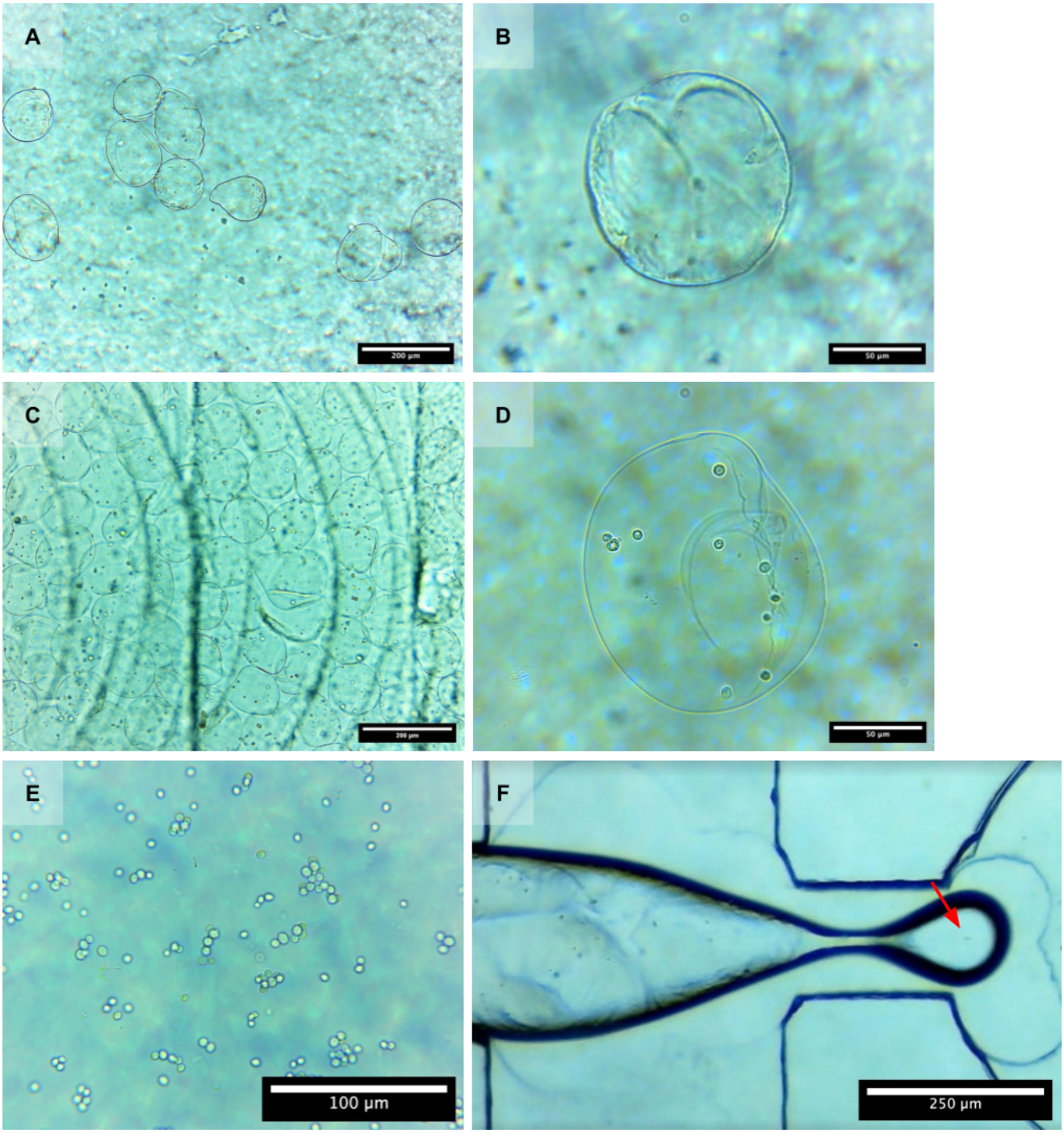

Figure 4: Micrographs of microparticles and yeast cells. (A) plain alginate microparticles at 10x, (B) 40x, (C) multiple alginate microparticles with yeast at 10x and; (D) an individual alginate microparticle with yeast at 10x. For individual size measurements, microparticles in images similar to Fig. 4A & 4C were isolated using the Segment Anything Model (SAM) as shown in Fig. S2. For counting and evaluation of yeast cell encapsulation, images similar to those in Fig. 4C & 4D were used. (E) Micrograph of *S. cerevisiae* yeast cells suspended in sucrose solution. Cell morphology and counts were checked prior to introduction into the alginate solution for microfluidic encapsulation. (F) Micrograph of an alginate-in-oil droplet formation. Multiple cells with the characteristic spherical-ovoid shape are visible in the alginate phase. A single cell was identified in the droplet being formed towards the end of the orifice.

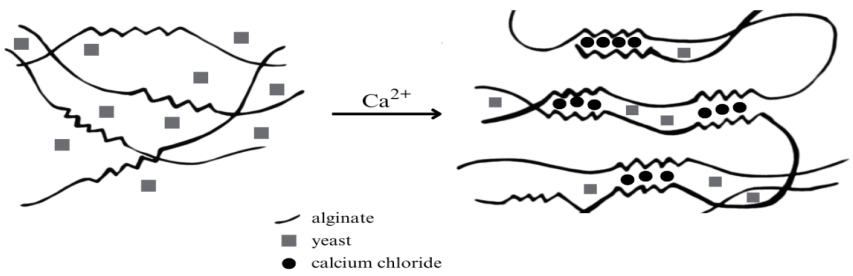

Figure 5: A schematic diagram of sodium alginate containing yeast cells when crosslinked with calcium ions.

To confirm the presence of encapsulated cells in the hydrogels, yeast cells from the stock solution were imaged under the microscope (**Fig. 4E**). The cells were spherical-ovoid in shape and had an average size of 5.36 µm, which was in agreement with data from literature (Chavez et al. 2024). The microparticles produced using alginate with yeast were confirmed to have cells of similar shape and size entrapped in the matrix. Microparticles imaged at 40x magnification were analyzed to determine the encapsulated yeast count, as seen in **Fig. 4D**. Considering the dilution of yeast stock in alginate, a count of 55 cells per µL was calculated for, theoretically resulting in 1 yeast cell being encapsulated for every 10 microparticles. However, multiple cell encapsulation was observed (**Fig. 4D**). On average, using manual counting, the microparticles contained 4 ± 2 yeast cells. A non-homogenous dispersion of cells in the alginate solution was likely due to the mode of mixing. Vortexing proved to be an inadequate method of evenly dispersing the cells in alginate due to the precursor's high viscosity. From the sample population, 30% of the microparticles analyzed were determined to have 4 yeast cells. When uptaking the alginate solution with yeast, it is likely that sections of the syringe contained a lower concentration of yeast than others. Use of the stir bar in the syringe increased dispersion within sections but did not result in successful distribution of the cells in the total volume of the solution uptaken. Increased homogeneity of cells in the alginate solution can be achieved with manual mixing using a sterile stirring rod or spatula (Hoesli et al. 2017). Additionally, with widefield imaging alone, it is not always possible to definitively determine whether a cell is embedded or simply adhered to the droplet exterior, particularly during or shortly after droplet formation. While great care was taken to reduce this possibility by imaging shortly after crosslinking, this cannot be ruled out entirely. Imaging methods, such as the use of confocal microscopy or electron microscopy, may be used in future studies to fully characterize the occurrence.

CONCLUSION

This study demonstrates a cost-effective CNC-milled microfluidic platform for producing alginate hydrogel microparticles and encapsulating *Saccharomyces cerevisiae*. The flow-focusing droplet generator produced reproducible droplets of consistent size and morphology dependent on flow parameters and device geometry; microscopy confirmed the successful encapsulation of yeast cells. However, the use of vortex mixing for the reported experiments resulted in non-uniform cell dispersion, suggesting that alternative mixing strategies may be necessary for more controlled, potentially single-cell, encapsulation.

While the study focused on the encapsulation mechanism, further investigation is needed to assess cell viability and function post-encapsulation. Future work will involve refining droplet generation parameters, improving cell mixing protocols, and conducting viability and metabolic activity assays. This work establishes a viable microfluidic encapsulation method using locally accessible fabrication techniques, demonstrating its feasibility for further development in the Philippines, where such approaches remain largely unexplored.

ACKNOWLEDGEMENT

This project is funded by the Department of Science and Technology (DOST) through the Science for Change Program (S4CP) – Niche Centers in the Regions for R&D (NICER) Grant: 8672 and monitored by Philippine Council for Health Research and Development (DOST-PCHRD). We would like to gratefully acknowledge the Integrated Protein Research & Development Center (IPRDC) for their materials and facilities, the Ateneo Research Institute of Science and Engineering (ARISE) for administrative and logistical support, the Ateneo de Manila University Department of Chemistry for the use of their reagents and the Department of Science and Technology Balik Scientist Program (DOST-BSP) for their continued support. We would also like to thank Ateneo de Manila University Biomolecular Research Group for the use of their hemocytometer and the Philippine Institute of Pure and Applied Chemistry (PIPAC) for the use of their laboratory facilities.

CONFLICT OF INTEREST

The authors declare that there is no conflict of interest.

CONTRIBUTIONS OF INDIVIDUAL AUTHORS

AMDH led the study, focusing on alginate bead fabrication, and conducted experiments alongside MFJPO, who specialized in microfluidics and was in charge of microfluidic device fabrication and design. These authors contributed equally to the manuscript. NAO provided guidance, and performed cell preparation, counting, and analysis. MDCA assisted in microfluidic design and supported MFJPO in experiments and image analysis. JNK and ADOD provided experimental support, assisted with data acquisition and analysis, and contributed to manuscript drafting. RJSG supervised the study, contributed to experimental design, and revised the manuscript. All authors discussed the results and contributed to the final manuscript.

REFERENCES

Ahn S, Kim G. Cell-encapsulating alginate microsized beads using an air-assisted atomization process to obtain a cell-laden hybrid scaffold. J Mater Chem B. 2015;3(47):9132-9139. doi:10.1039/C5TB01629K

Bonani W, Cagol N, Maniglio D. Alginate Hydrogels: A Tool for 3D Cell Encapsulation, Tissue Engineering, and Biofabrication. In: Chun HJ, Reis RL, Motta A, Khang G, eds. Biomimicked Biomaterials: Advances in Tissue Engineering and Regenerative Medicine. Springer; 2020:49-61. doi:10.1007/978-981-15-3262-7_4

Brousseau EB, Dimov SS, Pham DT. Some recent advances in multi-material micro- and nano-manufacturing. Int J Adv Manuf Technol. 2010;47(1-4):161-180. doi:10.1007/s00170-009-2214-5

Chavez CM, Groenewald M, Hulfachor AB, Kpurubu G, Huerta R, Hittinger CT, Rokas A. The cell morphological diversity of Saccharomycotina yeasts. FEMS Yeast Research. 2024;24:foad055. doi:10.1093/femsyr/foad055

Choudhary J, Singh S, Nain L. Thermotolerant fermenting yeasts for simultaneous saccharification fermentation of lignocellulosic biomass. Electronic Journal of Biotechnology. 2016;21:82-92. doi:10.1016/j.ejbt.2016.02.007

Collins DJ, Neild A, deMello A, Liu AQ, Ai Y. The Poisson distribution and beyond: methods for microfluidic droplet production and single cell encapsulation. Lab Chip. 2015;15(17):3439-3459. doi:10.1039/C5LC00614G

Gasperini L, Mano JF, Reis RL. Natural polymers for the microencapsulation of cells. J R Soc Interface. 2014;11(100):20140817. doi:10.1098/rsif.2014.0817

Giuliano C. Droplets encapsulation for biological applications: a review. Microfluidics Innovation Center. Accessed March 8, 2025. https://microfluidics-innovation-center.com/reviews/droplets-encapsulation-for-biological-applications-a-review/

Grace JR, Ebneyamini A. Connecting particle sphericity and circularity. Particuology. 2021;54:1-4. doi:10.1016/j.partic.2020.09.006

Guckenberger DJ, De Groot TE, Wan AMD, Beebe DJ, Young EWK. Micromilling: a method for ultra-rapid prototyping of plastic microfluidic devices. Lab Chip. 2015;15(11):2364-2378. doi:10.1039/C5LC00234F

Hamilton M, Harrington S, Dhar P, Stehno-Bittel L. Hyaluronic Acid Hydrogel Microspheres for Slow Release Stem Cell Delivery. ACS Biomater Sci Eng. 2021;7(8):3754-3763. doi:10.1021/acsbiomaterials.1c00658

Hoesli CA, Kiang RLJ, Mocinecová D, Speck M, Mošková DJ, Donald-Hague C, Lacík I, Kieffer TJ, Piret JM. Reversal of diabetes by βTC3 cells encapsulated in alginate beads generated by emulsion and internal gelation. Journal of Biomedical Materials Research Part B: Applied Biomaterials. 2012;100B(4):1017-1028. doi:10.1002/jbm.b.32667

Hoesli CA, Kiang RLJ, Raghuram K, et al. Mammalian Cell Encapsulation in Alginate Beads Using a Simple Stirred Vessel. Journal of Visualized Experiments (JoVE). 2017;(124):e55280. doi:10.3791/55280

Hu Y, Wang Q, Wang J, Zhu J, Wang H, Yang Y. Shape controllable microgel particles prepared by microfluidic combining external ionic crosslinking. Biomicrofluidics. 2012;6(2):026502. doi:10.1063/1.4720396

Inda ME, Lu TK. Microbes as Biosensors. Annu Rev Microbiol. 2020;74:337-359. doi:10.1146/annurev-micro-022620-081059

Karaca MA, Kancagi DD, Ozbek U, Ovali E, Gok O. Preparation of Cell-Loaded Microbeads as Stable and Injectable Delivery Platforms for Tissue Engineering. Biomimetics. 2023;8(2):155. doi:10.3390/biomimetics8020155

Khayambashi P, Iyer J, Pillai S, Upadhyay A, Zhang Y, Tran SD. Hydrogel Encapsulation of Mesenchymal Stem Cells and Their Derived Exosomes for Tissue Engineering. International Journal of Molecular Sciences. 2021;22(2):684. doi:10.3390/ijms22020684

Łabowska MB, Skrodzka M, Sicińska H, Michalak I, Detyna J. Influence of Cross-Linking Conditions on Drying Kinetics of Alginate Hydrogel. Gels. 2023;9(1):63. doi:10.3390/gels9010063

Lashkaripour A, Rodriguez C, Ortiz L, Densmore D. Performance tuning of microfluidic flow-focusing droplet generators. Lab on a Chip. 2019;19(6):1041-1053. doi:10.1039/C8LC01253A

Liga A, Morton JAS, Kersaudy-Kerhoas M. Safe and cost-effective rapid-prototyping of multilayer PMMA microfluidic devices. Microfluidics and Nanofluidics. 2016;20(12):1-12. doi:10.1007/s10404-016-1823-1

Macosko EZ, Basu A, Satija R, et al. Highly Parallel Genome-wide Expression Profiling of Individual Cells Using Nanoliter Droplets. Cell. 2015;161(5):1202-1214. doi:10.1016/j.cell.2015.05.002

McIntyre D, Lashkaripour A, Arguijo D, Fordyce P, Densmore D. Versatility and stability optimization of flow-focusing droplet generators via quality metric-driven design automation. Lab Chip. 2023;23(23):4997-5008. doi:10.1039/D3LC00189J

Mohanto S, Narayana S, Merai KP, Kumar JA, Bhunia A, Hani U, Fatease AA, Gowda BHJ, Nag S, Ahmed MG, Paul K, Vora LK. Advancements in gelatin-based hydrogel systems for biomedical applications: A state-of-the-art review. International Journal of Biological Macromolecules. 2023;253:127143. doi:10.1016/j.ijbiomac.2023.127143

Moragues T, Arguijo D, Beneyton T, Modavi C, Simutis K, Abate A, Beret JC, Demello A, Densmore D, Griffiths A. Droplet-based microfluidics. Nat Rev Methods Primers. 2023;3(1):1-22. doi:10.1038/s43586-023-00212-3

Pfreundt A, Andersen KB, Dimaki M, Svendsen WE. An easy-to-use microfluidic interconnection system to create quick and reversibly interfaced simple microfluidic devices. Journal of Micromechanics and Microengineering. 2015;25(11). doi:10.1088/0960-1317/25/11/115010

Ren K, Zhou J, Wu H. Materials for Microfluidic Chip Fabrication. Acc Chem Res. 2013;46(11):2396-2406. doi:10.1021/ar300314s

Rivera-Tarazona LK, Bhat VD, Kim H, Campbell ZT, Ware TH. Shape-morphing living composites. Science Advances. 2020;6(3):eaax8582. doi:10.1126/sciadv.aax8582

Rivera-Tarazona LK, Campbell ZT, Ware TH. Stimuli-responsive engineered living materials. Soft Matter. 2021;17(4):785-809. doi:10.1039/D0SM01905D

Sadasivan S, Pradeep S, Ramachandran JC, Narayan J, Gęca MJ. Advances in droplet microfluidics: a comprehensive review of innovations, morphology, dynamics, and applications. Microfluid Nanofluid. 2025;29(3):17. doi:10.1007/s10404-025-02789-5

Samokhin AS. Syringe Pump Created using 3D Printing Technology and Arduino Platform. J Anal Chem. 2020;75(3):416-421. doi:10.1134/S1061934820030156

Savić Gajić IM, Savić IM, Svirčev Z. Preparation and Characterization of Alginate Hydrogels with High Water-Retaining Capacity. Polymers. 2023;15(12):2592. doi:10.3390/polym15122592

Schneider T, Kreutz J, Chiu DT. The Potential Impact of Droplet Microfluidics in Biology. Anal Chem. 2013;85(7):3476-3482. doi:10.1021/ac400257c

Scott S, Ali Z. Fabrication Methods for Microfluidic Devices: An Overview. Micromachines. 2021;12(3):319. doi:10.3390/mi12030319

Serp D, Cantana E, Heinzen C, Von Stockar U, Marison IW. Characterization of an encapsulation device for the production of monodisperse alginate beads for cell immobilization. Biotechnology and Bioengineering. 2000;70(1):41-53. doi:10.1002/1097-0290(20001005)70:1<41::AID-BIT6>3.0.CO;2-U

Tomić SLj, Babić Radić MM, Vuković JS, Filipović VV, Nikodinovic-Runic J, Vukomanović M. Alginate-Based

Hydrogels and Scaffolds for Biomedical Applications. Mar Drugs. 2023;21(3):177. doi:10.3390/md21030177

Velders AH, Van Lieshout L, Brienen EAT, Diederich B, Saggiomo V. Step-by-step : A microfluidic (PDMS) staircase device for size sorting microparticles down to 25 µm using a 3D-printed mold. Published online August 14, 2023. doi:10.26434/chemrxiv-2023-fnhkr-v2

Xu J, Harasek M, Gföhler M. From Soft Lithography to 3D Printing: Current Status and Future of Microfluidic Device Fabrication. Polymers. 2025; 17(4):455. doi:10.3390/polym17040455

Zhang C, Grossier R, Candoni N, Veesler S. Preparation of alginate hydrogel microparticles by gelation introducing cross-linkers using droplet-based microfluidics: a review of methods. Biomaterials Research. 2021;25(1):41. doi:10.1186/s40824-021-00243-5

SUPPLEMENTARY INFORMATION

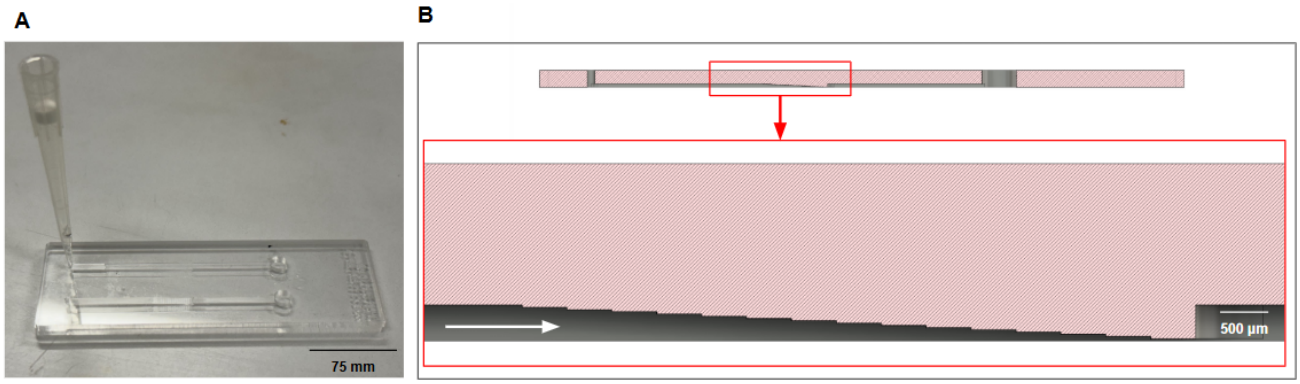

Figure S1: A microfluidic device for size-based separation of microparticles in suspension. (A) An image of the device in use. The inlet is sized to accept a 200-µL micropipette tip as a reservoir, while the outlet has a larger diameter to facilitate aspirating excess liquid after passing through the filter. (B) Cross-section view of the filter design. The detailed view shows the step filter which features (L-R) an initial inlet channel height of 400 µm, followed by shallower steps of 25 µm for every 0.5 mm along the channel length, ending in a 25 µm step before expanding back to 400 µm. Particles are carried along with the fluid flow (white arrow). Particles of different sizes are trapped in the respective steps.

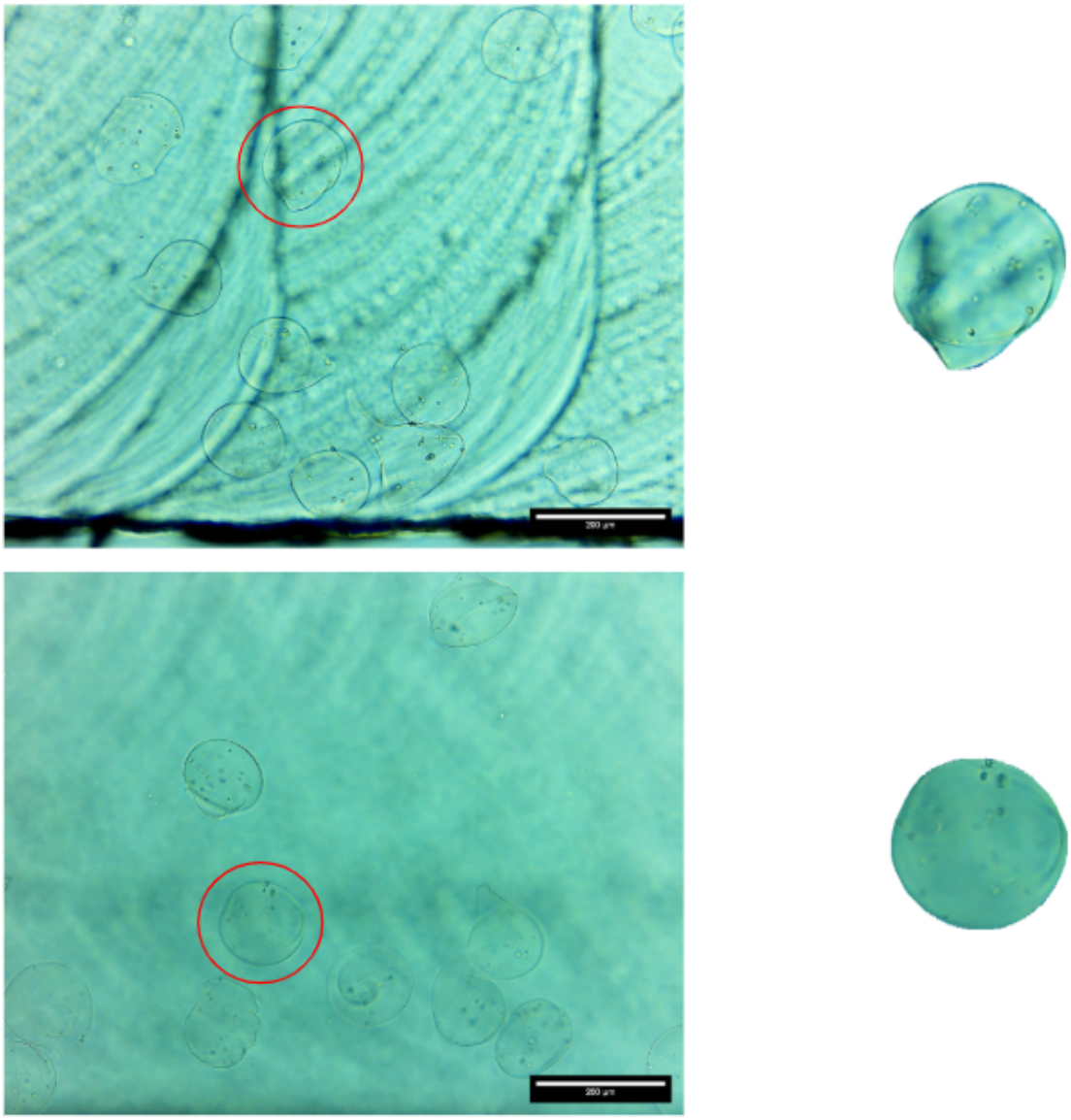

Figure S2: Micrographs of alginate microparticles taken at 10x for determining circularity. Images of 50 distinct particles were isolated using the Segment Anything Model (SAM). The threshold was adjusted to consider only the shape of the particle and eliminate any encapsulated yeast cells in the analysis.

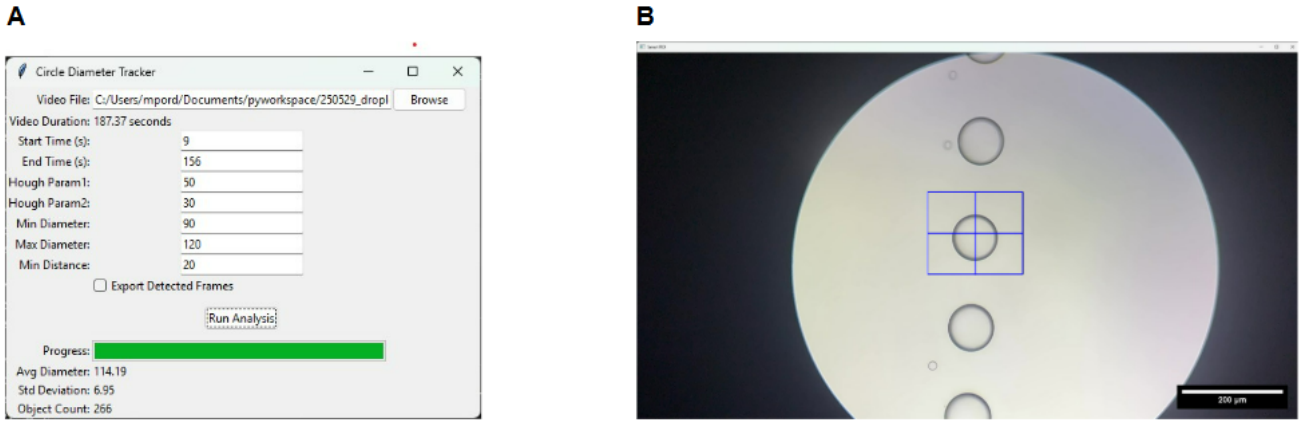

Figure S3: User interface during use of the developed droplet analysis script. (A) Settings window with video file selection and analysis parameters, including start and end time of droplet measurement, Hough circle analysis parameters, and cutoff of minimum and maximum diameter. (B) Still frame of 240 FPS slow-motion phone video with selected ROI (blue box).

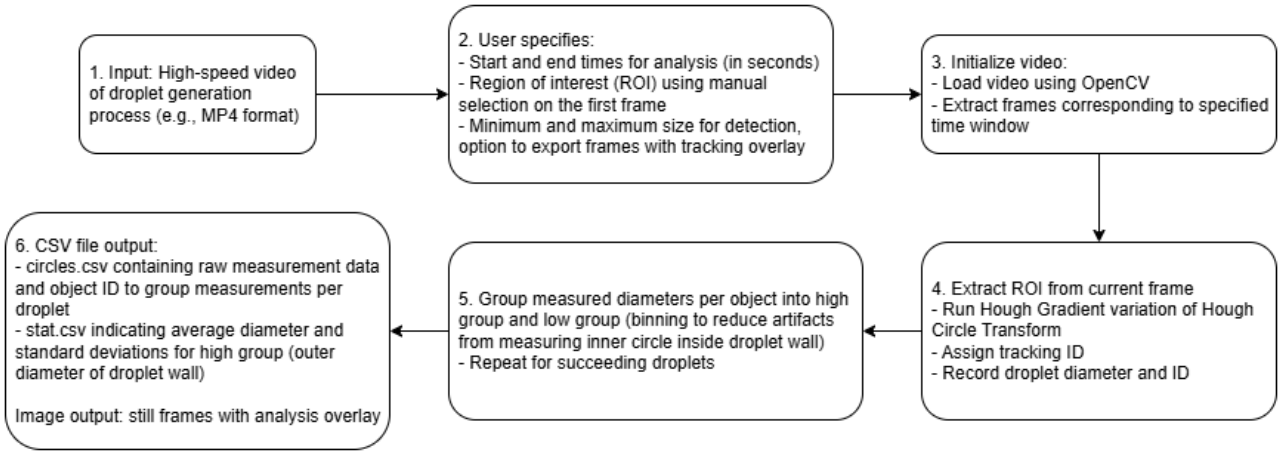

Figure S4: Flowchart for the dynamic droplet analysis image processing pipeline developed for analysis of high speed 240 FPS smartphone video. The user imports a high-speed video of the droplet generation process, then specifies the time period of analysis, a region of interest, and a scale factor. Image processing is conducted through OpenCV, then the droplet diameters and counts are exported into a CSV file along with annotated snapshots of the analyzed frames and basic statistical analysis over the series of frames.

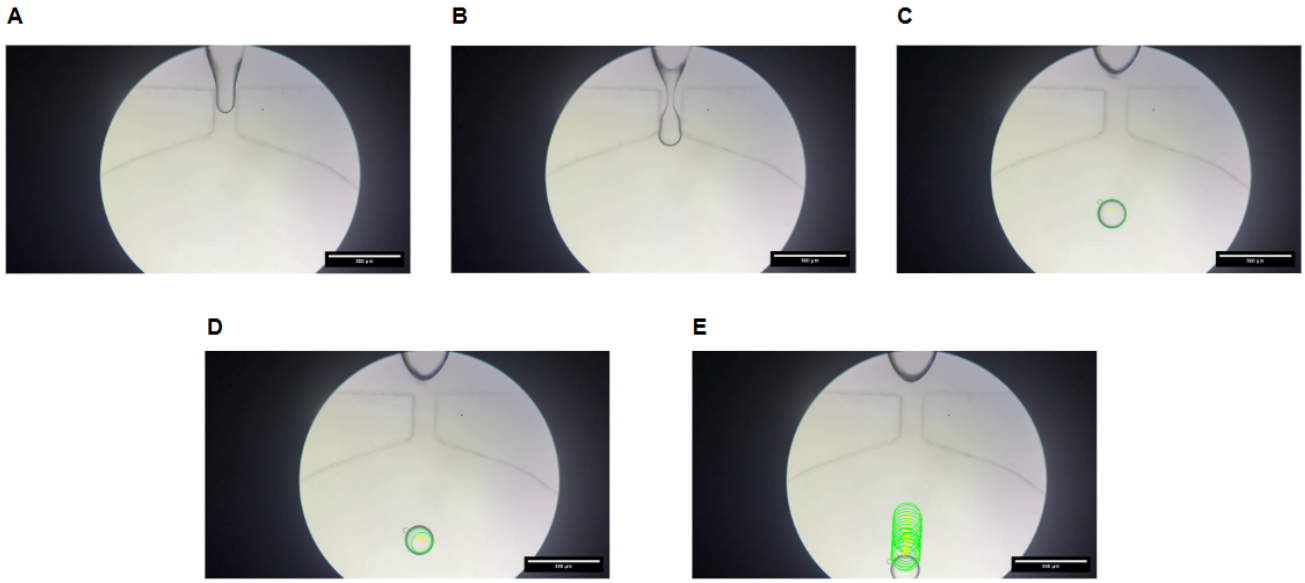

Figure S5: Still frames from video analysis script developed to process 240 FPS slow-motion smartphone footage showing microfluidic droplet formation. The script allows for a standard process of identifying droplet diameter in pixels, for subsequent conversion to microns. (A) Alginate phase entering junction prior to droplet formation.(B) Droplet formation without overlay. (C) Droplet enters region of interest and is identified by software (green overlay, ID:1). (D) Tracking error where a second droplet is marked by the software. (E) Droplet exits region of interest, summary of all measurements taken are displayed.

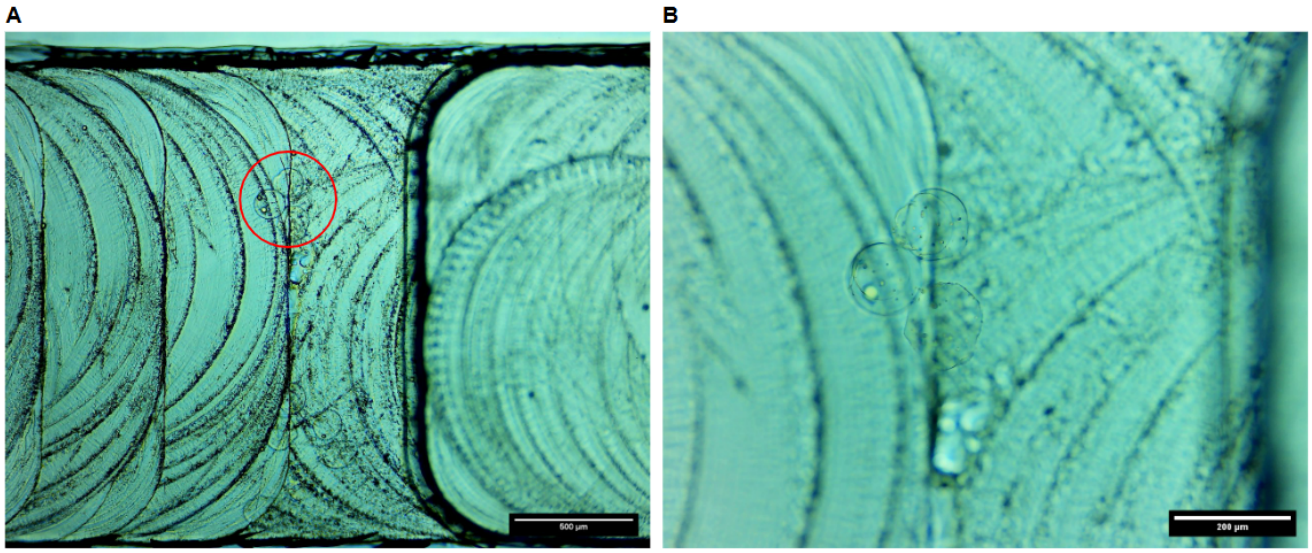

Figure S6: Microscope images of the microfluidic size-based particle separation device in use. (A) Image taken with a 4x objective with particles of interest encircled in red. (B) Image taken with a 10x objective with a clearer view of the crosslinked microparticles.

Table S1: Droplet diameter data at varying flow rates from 240 FPS slow-motion smartphone footage analyzed using developed video analysis script.

Alginate phase flow rate (µL/min)	Oil phase flow rate (µL/min)	Average droplet diameter (µm)	Standard deviation (µm)
1	40	222.13	3.76
1	60	194.74	2.39
1	80	170.13	4.20
1	100	173.08	7.06
1	120	156.93	8.51
1	140	150.79	8.39
1	160	144.04	5.31
1	180	155.29	7.90
1	200	125.20	3.78
1	250	182.97	3.31
1	500	173.08	7.07
2	200	160.07	4.35
3	300	173.85	8.08
4	400	175.46	8.88
5	500	170.57	6.98

Table S2: Initial particle diameter data using updated image processing methods for non-spherical particles

Maximum diameter (µm)	Minimum diameter (µm)
166.481	146.000
153.496	145.010
131.822	123.000
149.576	132.000
137.902	127.252
154.019	137.091
162.373	146.923
150.659	135.059
166.373	135.506
156.732	134.862
151.568	140.000
165.653	142.000
153.473	130.000
156.605	144.479
150.748	130.000
161.941	135.000
165.922	118.000

134.826	126.000
149.790	139.718
155.724	128.000
163.835	141.421
162.432	138.232
165.560	147.785
159.662	138.000
147.801	128.000
164.210	145.327
173.954	132.000
148.977	136.847
218.215	193.716
160.854	129.708
152.765	132.000
178.533	134.228
160.328	131.622
162.117	147.000
159.850	140.000
149.308	116.000
148.556	131.380
151.539	137.000
148.519	134.618
167.547	147.755
155.708	133.000
180.250	151.921
164.158	144.832
188.298	146.000
161.756	147.000
181.033	143.000
152.345	133.000
191.859	145.758
173.277	139.837
188.003	146.000

Particles measured here were initially filtered using a microfluidic size-sorting device, imaged, then masked using the Segment Anything Model (SAM), followed by particle analysis in ImageJ to determine the Feret diameter (major and minor)